Coregistered tomographic x-ray and optical breast imaging: initial results

Quan Zhang
Harvard Medical School
Massachusetts General Hospital
The Martinos Center for Biomedical Imaging
13th Street, Building 149, Room 2301
Charlestown, Massachusetts 02129
E-mail: qzhang@nmr.mgn.harvard.edu

Thomas J. Brukilacchio
Innovations in Optics, Inc.
Woburn, Massachusetts 01801

Ang Li
Tufts University
Physics Dept
Medford, Massachusetts 02155

Jonathan J. Stott
Tina Chaves
Elizabeth Hillman
Harvard Medical School
Massachusetts General Hospital
The Martinos Center for Biomedical Imaging
13th Street, Building 149, Room 2301
Charlestown, Massachusetts 02129

Tao Wu
MaryAnn Chorlton
Elizabeth Rafferty
Richard H. Moore
Daniel B. Kopans
Harvard Medical School
Massachusetts General Hospital
The Breast Imaging Unit
Boston, Massachusetts 02114

David A. Boas
Harvard Medical School
Massachusetts General Hospital
The Martinos Center for Biomedical Imaging
13th Street, Building 149, Room 2301
Charlestown, Massachusetts 02129

Abstract. We describe what is, to the best of our knowledge, the first pilot study of coregistered tomographic x-ray and optical breast imaging. The purpose of this pilot study is to develop both hardware and data processing algorithms for a multimodality imaging method that provides information that neither x-ray nor diffuse optical tomography (DOT) can provide alone. We present in detail the instrumentation and algorithms developed for this multimodality imaging. We also present results from our initial pilot clinical tests. These results demonstrate that strictly coregistered x-ray and optical images enable a detailed comparison of the two images. This comparison will ultimately lead to a better understanding of the relationship between the functional contrast afforded by optical imaging and the structural contrast provided by x-ray imaging. © *2005 Society of Photo-Optical Instrumentation Engineers.* [DOI: 10.1117/1.1899183]

1 Introduction: Significance of Combining X-Ray and Optical Breast Imaging

Diffuse optical tomography (DOT) is a relatively new breast imaging modality.[1–8] Unlike the diaphanoscopy used in the 1930s through the 1980s, which attempted to image breast tumors by simply looking at the shadows of light transmitted through the breast,[9,10] DOT uses tomography to reconstruct 3-D images of the entire breast volume, reducing the opportunities for overlapping structures to be falsely diagnosed as cancer. DOT also has the potential to provide physiological or pathological information about the breast; e.g., via determina-

tion of both the absorbing and scattering structures, or by utilizing spectroscopic analysis to determine blood volume and oxygen saturation, water, and lipid distributions in the breast. With DOT, the breast is illuminated with near-IR laser light of different wavelengths, and the multiply scattered light that exits the tissue is measured using a sensitive photodetector. Light traveling through the tissue is modeled using the diffusion approximation to the radiative transport equation.[11] With appropriate source and detector arrays, images of the breast can be tomographically reconstructed at each wavelength (*in vivo* optical absorption and scattering coefficients of the breast are the parameters reconstructed in the images). From the spectroscopic information acquired through the combination of multiple wavelengths, total hemoglobin con-

---

Address all correspondence to Dr. Quan Zhang, Harvard Medical School, Massachusetts General Hospital, The Martinos Center for Biomedical Imaging, 135h Stree, Building 149, Room 2301, Charlestown, Massachusetts 02129. E-mail: qzhang@nmr.mgh.harvard.edu
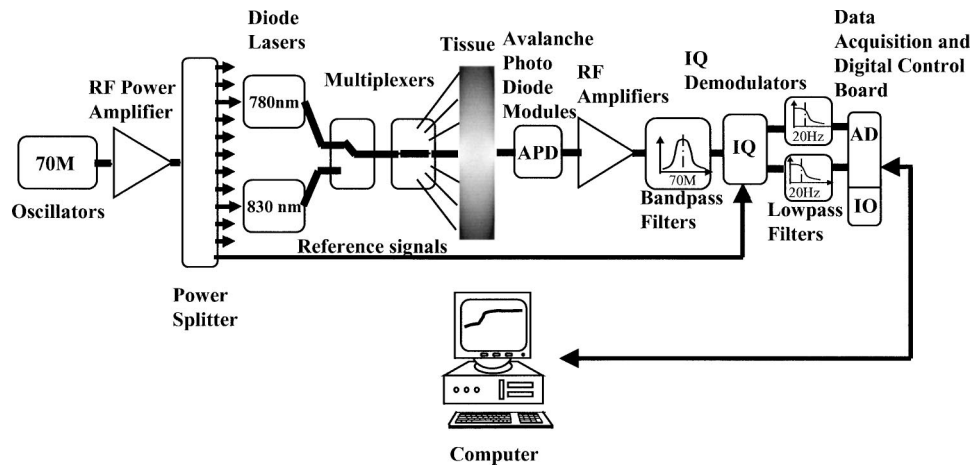
Fig. 1 Structure of the RF imager: signal flow from one source location to one detector (for simplicity the other eight detector channels are not shown).

centration and oxygen saturation, water, and lipid distributions over the tissue in the reconstructed image can then be calculated quantitatively. Diagnosis of breast lesions using DOT is based on the assumption that pathological tissue changes affect the local blood supply, oxygen consumption status, and other parameters reflected through the optical properties, such as water content and scattering, thereby generating optical contrast. Thus far, pilot *in vivo* bulk optical properties of breast tissue[12,13] and *in vivo* measurements of endogenous optical properties and endogenous tumor contrast have been reported.[5–8,13–26] The use of dynamic features[27] and exogeneous contrast agents[28,29] have also been investigated. In addition to using optical imaging as a stand-alone modality, optical imaging guided by ultrasound[30,31] and magnetic resonance imaging[32] (MRI) has also been tested.

X-ray imaging (mammography) is currently the most widely accepted method for the diagnosis of breast lesions. Mammography screening is the most effective means of detecting early stage, nonpalpable breast cancers and has been shown clinically to reduce patient mortality through the early detection of breast cancers.[33,34] Studies have shown[35–37] the sensitivity of mammography to be about 86%, and screening for breast cancer improves early detection of aggressive cancers that may reduce a woman's life expectancy.[38] However, further improvements and multimodality imaging (coregistered optical and X-ray imaging in our case) are still required. For example, x-ray breast imaging reveals only morphologic information. It does not provide physiological data, is generally nonspecific, and involves ionizing radiation. MRI or ultrasound can be used as adjunctive tests, but they have limited specificity.[39] In addition, the high cost of MRI discourages its widespread use in screening. DOT, on the other hand, is inexpensive, provides relevant physiological information, and is nonionizing and noninvasive. DOT, however, suffers from relatively low spatial resolution. By combining x-ray and diffuse optical imaging techniques we hope to create a multimodality imaging method that combines the benefits of both. We anticipate that the combined method will have increased sensitivity as DOT may detect lesions missed by x-ray imaging alone, and increased specificity may result from the additional functional information that DOT could provide in the interpretation of x-ray images.

In the following sections we present our work on combining x-ray and optical breast imaging. First we present the instrumentation, followed by a discussion of the algorithms we utilize for processing the combined data sets. Preliminary clinical experimental results are then shown to demonstrate the feasibility of this method.

To the best of our knowledge, this is the first study of coregistered tomographic x-ray and optical breast imaging. Through this initial work, we demonstrate that coregistered x-ray and optical breast imaging is feasible and enables a direct comparison of optical images with x-ray images. Previous studies on optical breast imaging have compared DOT and x-ray images obtained at separate times.[7,14] This approach, however, does not provide a true coregistration of the contrast seen in each method since the positioning of the breast can differ by a few centimeters, consequently confounding the interpretation of the images. With our combined x-ray/DOT breast imaging approach, the images are from the same compressed breast (with x-ray fiducials to guarantee the alignment) and are collected sequentially within a period of 90 s. This coregistration will ultimately enable a better understanding of the relationship between x-ray measures of morphology and optical measures of tissue physiology.

2 Instrumentation

The frequency domain optical imaging system uses a 70-MHz radio frequency (RF) modulation of the optical signal and homodyne detection[40,41] for its data collection. It has been integrated with a tomosynthesis,[42] a prototype 3-D digital mammography system, and both optical and x-ray measurements are collected for the same subject. Essential to coregistration of the DOT and x-ray images is our optical probe design.

2.1 The RF Imaging System

The RF imaging system employs in-phase and quadrature-phase (IQ) demodulation techniques first introduced for DOT

by Yang et al.[40] and Chance et al.[41] Our system uses two diode laser sources (785 and 830 nm, respectively), time-shared between 40 source fibers and nine avalanche photodiode (APD, Hamamatsu C5331-04) detector channels. Figure 1 is a block diagram of the signal flow from one source location to one detector (for simplicity the other eight detector channels are not shown). On the source side, the incident laser light is modulated at a frequency of 70 MHz. A 2×1 optical multiplexer selects one of the two source lasers and a 1×40 optical multiplexer (Dicon Fiberoptics VX500) switches the laser between 40 source positions (using 140-μm multimode silica fibers). On the detector side, light emerging from the medium is collected by avalanche photodiodes (Hamamatsu C5331-04, through 3-mm-diam silica fiber bundle), converted to a voltage, amplified and then demodulated. Demodulated I and Q voltages are sampled by two 16-bit analog-to-digital (AD) boards, from which the amplitudes and the phases are calculated. The computer controls the operation of the imager through its digital input-output (IO) interface. Typical characterization results of this imager are as follows: Noise equivalent power (NEP): 1 pW/Hz$^{1/2}$; maximum bandwidth: 20 Hz; modulation depth: roughly 75%; output light power at the end of the source fiber: approximately 8 mW; dynamic range: 60 dB; amplitude-phase crosstalk: 0.02 deg/dB; time to complete data collection for one image: 60 s; maximum single channel (dual wavelength) sampling rate: 12 Hz (limited by the 2×1 optical multiplexer).

2.2 Optical Probe and System Setup

Our optical breast imaging probe design (shown in Fig. 2) is the essential component for coregistration of DOT and x-ray images (manufactured by Innovations in Optics, Inc). The optical probe should enable collection of the optical measurements without interfering with the x-ray image and without altering the position of the breast between acquisition of the optical and x-ray images. Ideally, the optical and x-ray images would be acquired simultaneously. However, we could not yet justify fabrication of an optical probe that was x-ray transparent, or at least spatially uniform to the x-ray image. We therefore designed a quick-release optical probe that enabled the x-ray images to be acquired immediately after the optical images (optical and x-ray images are acquired sequentially within 90 s) without moving the breast. The lower optical probe assembly, which sits on top of the x-ray digital detector housing, is comprised of a removable source fiber array and an inverted polycarbonate compression plate (the index of refraction at 800 nm is 1.573). The upper assembly consists of a standard compression plate modified to house a removable array of detection fibers. The 2.3-mm-thick and antireflection-coated compression plates remain stationary during both DOT and x-ray image acquisition. Metal markers at the edge of the compression plate with a fixed position relative to the optodes are used to ensure the strict coregistration of the two imaging modalities. The optical fiber arrays are quickly removed between the optical image and the x-ray image to reduce fiber induced artifact in the x-ray images. Removal of the fiber arrays does not alter the position of the breast tissue.

The 3-D x-ray images are generated using the tomosynthesis digital breast imaging system.[42,43] The tomosynthesis system uses an amorphous Si-based flat-panel detector located in the same position as the film cassette of a conventional film-
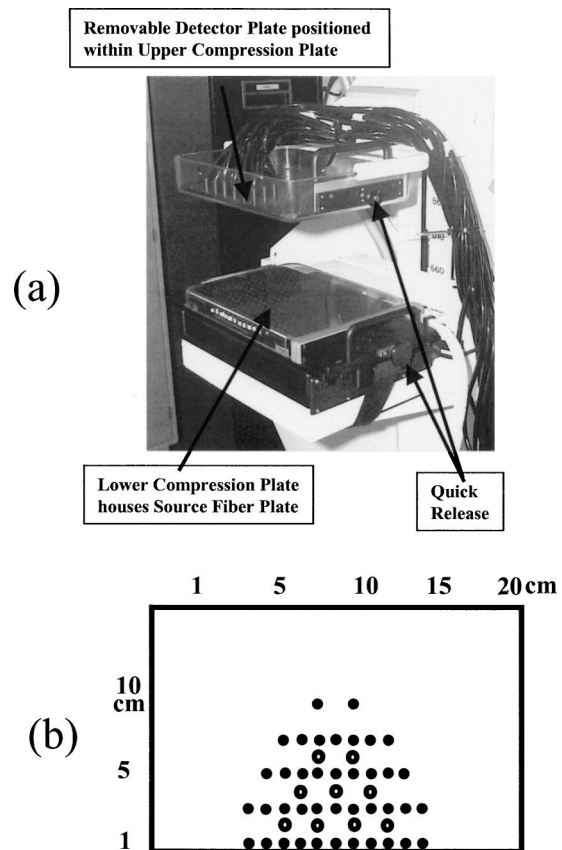

Fig. 2 (a) Structure of the compression plate designed for coregistered x-ray and optical breast imaging and (b) probe configuration. The solid circles indicate the location of source fibers and the open circles indicate the location of detector fibers. Source fibers and detector fibers are on the bottom and top plates, respectively, and are on a 1-cm grid.

screen mammography system. The detector has 1800×2304 pixels with a 100-μm pixel size. The tomosynthesis system reconstructs the 3-D structure of the breast using eleven projections taken over a 50-deg angular range above the base in 5-deg angular steps. The tomosynthesis images are reconstructed using a maximum likelihood iterative algorithm.[43] This x-ray system is ideal for our application, as it enables direct comparison of the 3-D structure of the breast. However, our optical imager could also be incorporated into a traditional 2-D x-ray mammography system. The combined x-ray and optical imaging system is shown in Fig. 3.

Initially, both the source and detector fiber arrays are placed within their respective compression plates. The patient is then positioned and compressed according to standard mammography procedures. The DOT image is acquired in less than 60 s. Immediately following DOT image acquisition both the source and the detector fiber arrays are removed using built-in quick release mechanisms. Finally, without moving the patient, an x-ray image is made. The entire procedure of DOT and x-ray image acquisition takes less than 90 s. This arrangement allows for strict coregistration of DOT and x-ray images.
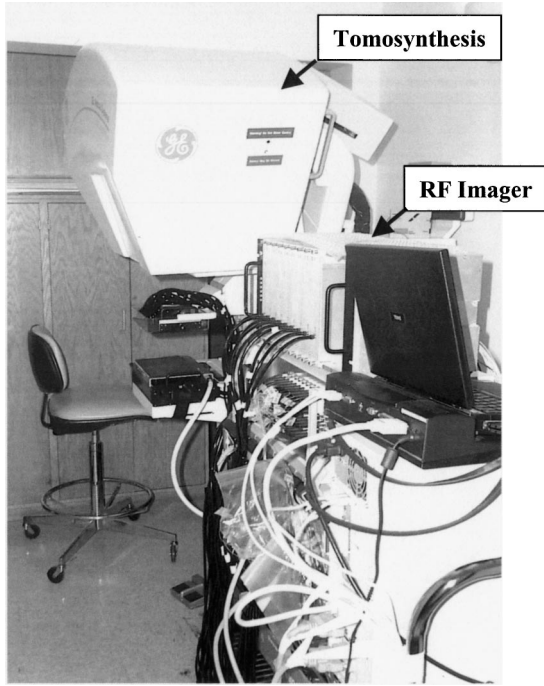
Fig. 3 Combined x-ray and optical imaging system. The RF imaging system is connected with the Tomosynthesis.

3 Algorithms

3.1 General Linear DOT Image Reconstruction Techniques

3.1.1 Forward modeling

Currently, the diffusion approximation to the radiative transport equation (diffusion model) is the most popular physical model used to describe photon propagation in highly scattering media.[2,44,45] In the frequency domain, we set the source term $S(\mathbf{r},t) = S(\mathbf{r})e^{i\omega t}$, where ω is the frequency and $\mathbf{r}$ is the position vector, and the photon fluence rate $\phi(\mathbf{r},t) = \Phi(\mathbf{r})e^{i\omega t}$, so that the diffusion equation with spatially uniform (i.e., homogeneous) optical properties becomes a Helmholtz equation

$$\left(\nabla^2 - \frac{v\mu_{a,0} + i\omega}{D_0}\right)\Phi_0(\mathbf{r}) = -\frac{1}{D_0}S(\mathbf{r}), \quad (1)$$

where μ_a is the absorption coefficient, $D = v/3(\mu'_s + \mu_a) \approx v/3\mu'_s$ and μ'_s is the reduced scattering coefficient, v is the speed of light in the medium, and the subscript 0 indicates unperturbed optical properties.

When the medium is heterogeneous μ_a is a function of position $\mathbf{r}$, and is the quantities that we would like to image. For image reconstruction using a linear perturbation approach, a solution to the inhomogeneous diffusion equation with an appropriate boundary condition is required. In the Rytov approximation,[46] the fluence rate is written as $\phi(\mathbf{r}) = \phi_0(\mathbf{r})e^{\psi(\mathbf{r})}$, where ϕ_0 is the incident field and ψ is the scattered wave. For a small absorbing inhomogeneity $\mu_a(\mathbf{r}) = \mu_{a0} + \delta\mu_a(\mathbf{r})$, where μ_{a0} is the constant background absorption coefficient (bulk optical property) and $\delta\mu_a(\mathbf{r})$ is the inhomogeneity term, the diffusion equation can be solved as

$$\psi_a = -\frac{1}{\phi_0(\mathbf{r}_s,\mathbf{r}_d)}\int G(\mathbf{r},\mathbf{r}_d)\frac{v\,\delta\mu_a(\mathbf{r})}{D_0}\phi_0(\mathbf{r}_s,\mathbf{r})d^3\mathbf{r}, \quad (2)$$

where G is the frequency domain Green's function,[2,44,45] the analytical solution, by using image sources, for a slab geometry with infinite X and Y dimensions, and ψ_a is the scattered wave produced by an absorption perturbation. The subscript s indicates sources and subscript d indicates detectors.

Equation (2) can be discretized to yield the following system of linear equations

$$\boldsymbol{\psi}_a = \mathbf{A}_a\delta\boldsymbol{\mu}_a, \quad (3)$$

where $\boldsymbol{\psi}_a$ is column vector with the scattered wave for each source-detector pair, $\mathbf{A}_a$ is the Jacobian or sensitivity matrix for the absorption inhomogeneity where the components of $\mathbf{A}_a$ are derived from the integrand of Eq. (2), and $\delta\boldsymbol{\mu}_a$ is a vector describing the absorption change at each voxel in the medium.

3.1.2 Inverse problem

The inversion of the linear system described in Eq. (3) is both ill-posed and (usually) underdetermined. Some type of regularization or stabilization technique is therefore required to obtain physically meaningful results. Different techniques to solve ill-posed linear systems have been studied.[44,47,48] These include algebraic methods, such as the algebraic reconstruction technique (ART) and the simultaneous iterative reconstruction technique[49] (SIRT), and subspace techniques such as truncated singular-value decomposition (TSVD) and the truncated conjugate gradient (TCG) algorithm.[50] Here we use the classic Tikhonov regularization approach.[51] If we abbreviate the linear system of Eq. (3) to a general form of $\mathbf{y} = \mathbf{Ax}$, the solution can be found, in a least-squares sense, as the functional minimization of the cost function

$$f(x) = \|\mathbf{y} - \mathbf{A}\cdot\mathbf{x}\|^2 + \lambda\|\mathbf{x}\|^2, \quad (4)$$

where $\lambda \geq 0$ is the regularization parameter. This minimization is known as Tikhonov regularization. By varying λ we select between fidelity to the measurements ($\lambda \to 0$) and small image norm ($\lambda \to \infty$). Equation (4) is minimized for a given λ by

$$\mathbf{x} = [\mathbf{A}^T\cdot\mathbf{A} + \mathbf{I}\cdot\lambda]^{-1}\mathbf{A}^T\mathbf{y}, \quad (5)$$

or under general assumptions

$$\mathbf{x} = \mathbf{A}^T[\mathbf{A}\cdot\mathbf{A}^T + \mathbf{I}\cdot\lambda]^{-1}\mathbf{y}. \quad (6)$$

We can use an L-curve technique to choose the regularization parameter λ in the Tikhonov regularization.[48,52] This involves plotting the curve of image norm versus residual parametrically versus the regularization parameter and choosing the value of α at the elbow of the curve. Here $\lambda = \alpha M$ and M is the maximum value of all the elements in $\mathbf{A}^T\mathbf{A}$. However, in practice the regularization parameter λ was chosen experimentally and was larger than that determined by the elbow of the L-curve to smooth image artifacts caused by significant model error in our reconstructions. As we discuss in the fol-

lowing, these model errors arise from treating the breast as a homogeneous slab and potentially light piping within the plastic plate compressing the breast.

3.2 Choosing the Reconstruction Area

Since the boundary is known from the 3-D x-ray images, this information can be used in determining the image reconstruction area, for instance we do not want to reconstruct optical properties outside or near the air-tissue boundary. In practice, we choose the region that is confined to the breast outline and covered by the source and detector arrays. In the image reconstruction, this constrains the absorption perturbation to this region within the breast only, and we are assuming that this is the area probed by our measurements.

Previous studies have shown that combing the *a priori* structural information from other imaging modality improves image quality.[53–56] *A priori* x-ray images can provide well-defined regions of interest (ROIs), where there is a high possibility of cancer or some other source of optical contrast. This *a priori* information can be incorporated into the DOT image reconstruction as a constraint with which to fine-tune the optical images. Spatial regularization for DOT was first introduced by Arridge and Schweiger[57] and elaborated in Pogue et al.[58] We previously described[59] the incorporation of prior x-ray spatial information provided into DOT. Here, we only use prior information from the x-ray image only, to define the volume of tissue in which we perform the image reconstruction to ensure that we are not reconstructing absorption contrast outside of the tissue. However, we still treat the breast as a slab geometry, which will introduce model error near the boundaries. Furthermore, we do not use the internal tissue structural information provided by x-ray imaging to constrain DOT as we have done previously.[59]

3.3 Estimating the Average Bulk Optical Properties of the Medium

Our described image reconstruction algorithm relies on an estimate of the average bulk optical properties of the medium. These optical properties are calculated in the following way. The first step is a phantom-based system calibration. The source and the detector coefficients are calibrated using homogeneous phantoms using the methodology described in Ref. 60. The homogeneous phantoms were soft bags filled with intralipid and ink solution. The phantom tests and the patient test were conducted under similar test conditions (phantom tests were done immediately after the patient test and with the same source-detector separations and the signal level acquired from the homogeneous phantoms were close to that acquired from the patient). These source and detector coefficients are used to calibrate the patient data. Repeated phantom tests indicated that the estimated source and detector coefficients were repeatable to within 5%. For the calibrated patient data, each frequency domain measurement from a specific source-detector pair is fit by the homogeneous diffusion model described in the algorithm section using a simplex-based nonlinear fit to determine the absorption coefficient and the reduced scattering coefficient. Recall that measurements are only obtained at 70 MHz. The average of these optical properties for all measurements (total number of measurements equals to the number of sources times the number of
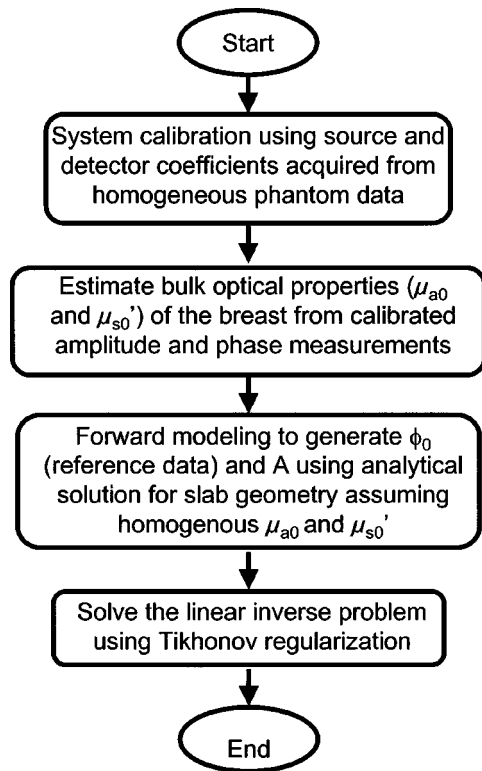

Fig. 4 Optical image reconstruction process flow chart.

detectors) is then calculated, and is taken as the average bulk optical properties of the breast. Figure 4 shows a schematic representation of the basic reconstruction procedure.

4 Preliminary Clinical Results

Determination of the *in vivo* optical properties of human breast tissue, as well as DOT-based breast imaging, has increasingly become a focus of researchers.[5,6,8,13,15,17–26] The purpose of our preliminary clinical study was to test our multimodality imaging methodology and identify shortcomings to improve on for a more rigorous future clinical study.

Before applying a new instrument to clinical measurements, it is important to verify its performance on tissue phantoms. The application of the described analysis algorithms provided estimates of the homogenous optical properties of phantoms accurate to within 10%. This accuracy has been verified for optical properties ranging $4\,\mathrm{cm}^{-1}<\mu_s'<12\,\mathrm{cm}^{-1}$ and $0.02\,\mathrm{cm}^{-1}<\mu_a<0.1\,\mathrm{cm}^{-1}$, typical of the published breast optical properties.[5,6,8,13,15,17–26] Heterogeneous phantoms with 2-cm-diam spherical tumors embedded in the center of a 5-cm-thick otherwise homogeneous slab were used to test the accuracy of the linear reconstruction procedure. The absorption contrast of the tumor, where we define the contrast as the difference between the tumor and the background, was always underestimated due to the point spread function (or blurring) of the inverse problem. The phantoms typically reconstructed 26% of the true contrast with a regularization $\alpha=0.02$ [Eq. (6)]. When we increased the regularization to $\alpha=0.8$ (as used for the clinical data), the reconstructed contrast was 1% of the true value. This underestimation of the true contrast can only be improved by pro-
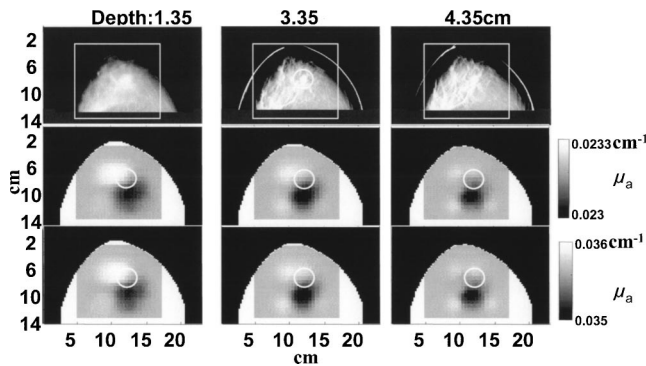
Fig. 5 For subject 1, slices of tomosynthesis, 785-nm optical absorption, and 830-nm absorption images are shown in the first, second, and third rows, respectively. The circle in the 3-D x-ray image indicates the location of the fibroadenoma. The white circle in the optical images indicates the lateral position of the lesion observed in the x-ray image. The rectangular area inside the breast is where the optical image reconstructions are confined.

viding prior information.[61] Li et al.[59] described the use of x-ray contrast as a prior for the optical image reconstruction and showed an improvement in the reconstructed absorption contrast accuracy. Further improvement in the reconstruction accuracy is left for future research. Nonetheless these phantom results indicated that our instrument was performing as expected and thus motivated the pilot clinical study.

In total, we measured 18 patients, aged 49 to 79, all of whom were scheduled for biopsy for the suspicious findings in a previous mammogram. Our goal was to determine whether the lesion diagnosed by x-ray imaging could also be detected in the reconstructed optical images. Of all the patients we studied, 14 cases provided useful information for our study; others were less useful because of various technical problems (often because our relatively small fiber optic probe failed to cover the lesion area). For these 14 patients, the x-ray images indicated that eight of them had a lesion smaller than 1 mm, such as microcalcifications (group A), for three patients the size ranged from 5 to 10 mm (group B), and for the other three the size ranged from 10 to 16 mm (group C). The cases presented below are for a subject from group B(case 2) and a subject from group C(case 1).

4.1 Case 1

A 49-yr-old female with a fibroadenoma (a benign lesion) 11×16 mm in size was examined by the coregistered optical and tomosynthesis imaging system. The reconstructed absorption images are shown in Fig. 5. The breast was compressed to a thickness of 5.9 cm. The regularization parameter used here was 0.8 times the maximum of $\mathbf{A}^T\mathbf{A}$. This large regularization parameter overcomes our measurement and modeling errors and results in significant smoothing of the data. The matrix size was 360 measurements by 6300 voxels.

From the x-ray result we can see the fibroadenoma, whose location was confirmed by our collaborating mammographer, and also more structure can be found on the left half of the breast, which indicates denser glandular tissue or connective tissue content than the right half.

The optical images reveal a region of increased absorption that corresponds with the location of the fibroadenoma. Com-

pared with the 3-D x-ray images, the optical contrast of the fibroadenoma is shifted by 2.5 cm. This may be due to the model mismatch between the real boundary of the breast and the simplified slab model used in the reconstruction. The large regularization parameter can also lead to significant bias error in the centroid location of the reconstructed absorbing perturbation.

The reduced absorption in the center and toward the right is consistent with the reduced x-ray density on the right half of the breast. However, it may also be due, in part, to distortions and artifacts due to the effects of the true boundary of the breast compared to our slab model, or due to other systematic errors that are unique to clinical data acquisition. The quantitative value of the average absorption coefficient shown in Fig. 5 is reasonable for a compressed breast. The spatial variation in the absorption coefficient is, we believe, significantly underestimated because of significant image smoothing caused by the large regularization parameter. For a regularization of $\alpha=0.8$, our phantom studies indicated that the reconstructed contrast was 1% of the true contrast. We expect the same reduction for the clinical studies, indicating that the true contrast of the fibroadenoma is more likely of the order of 0.01 cm^{-1} rather than 0.0001 cm^{-1}.

The difference between the estimated μ_a of the lesion for 785 and 830 nm is encouraging. Commonalties between absorbing regions in the two images indicate regions of high blood volume. Differences imply regions of oxygen saturation contrast. Other researchers have reported higher blood volume and lower oxygen saturation for benign breast lesions,[20] although further work is required to quantitatively compare our result with this finding.

4.2 Case 2

The patient was 65 yr old. The 3-D x-ray images revealed a vague density in the outer part of the left breast. After an excisional biopsy, performed after the optical image, pathology showed an invasive carcinoma of mucinous type (malignant breast lesion), 10×8.9 mm in size. There was also a radio dense, crescent-shaped area surrounding the lesion. The breast was compressed (full mammographic compression) to a thickness of 6.2 cm. The absorption images are shown in Fig. 6.

Close to the lesion location, indicated by the circle, an absorption contrast is present at both wavelengths. The systematic deviation in the position of the peak optical absorption contrast in the lateral coordinates relative to the position of the invasive carcinoma in the x-ray image could arise from modeling error or the large image regularization, as discussed for case 1. The deviation in the position also corresponds with the pattern of dense tissue observed in the x-ray image. A region of low contrast is again seen toward the center of the breast. As with case 1, this corresponds with the region of less x-ray dense tissue.

From these two cases we see that optical absorption contrast is greater near the benign and malignant lesions as well as in dense fibroglandular tissue identified on the 3-D x-ray image. These results provide a preliminary study of the correlation between x-ray and near-IR optical density. The other cases from groups B and C showed similar absorption contrast colocalized with the x-ray position of the lesion as well as image artifacts introduced presumably from modeling error
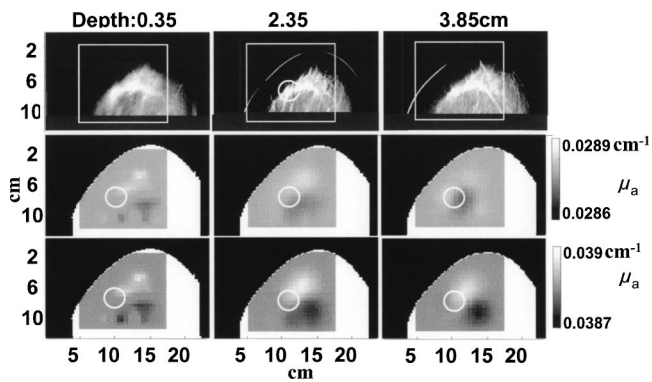
Fig. 6 For subject 2, slices of tomosynthesis, 785-nm optical absorption, and 830-nm absorption images are shown in the first, second, and third rows, respectively. The contrast in the x-ray image indicates the invasive carcinoma. The circle in the 3-D x-ray image indicates the location of the invasive tumor. The white circle in the optical images indicates the lateral position of the lesion observed in the x-ray image. The rectangular area inside the breast is where the optical image reconstructions are confined.

introduced by the air-tissue boundary. Examples from group A, with lesions smaller than 1 mm, were presumably too small to image given our current level of image noise and image artifacts.

5 Summary

We presented a new hybrid optical and x-ray mammography imaging system, together with an image reconstruction technique suitable for imaging the breast. Initial clinical results of the first coregistered optical and x-ray breast imaging were then presented. Optical images were reconstructed for both benign and malignant lesions, revealing optical contrast close to the location of the lesions shown in the corresponding x-ray images.

Without the help of the coregistered x-ray image, we would not have been able to determine which optical contrast derives from the breast lesion rather than from other tissue structures or is due to image artifact. In the optical images, we found that optical contrast may appear outside the region where the x-ray image indicates a lesion. Some of these regions of optical contrast may be physiological (e.g., dense tissue), others may be artifacts from undiagnosed systematic errors. This method of coregistration is significant for the direct comparison of diffuse optical breast images with the gold standard x-ray mammography, as it will guide interpretation and validation of the optical method.

Most of the lesions we imaged were small in size, and thus provided a low contrast-to-noise ratio. From the literature, we found that almost all clinical optical imaging results published previously were from lesions larger than 1.0 cm (Refs. 5 to 7 and 14), with a large portion of the images published for breast lesions around 3 cm in size. Most of our lesions were smaller than those published results.

With our current system, our image contrast-to-noise ratio is limited by modeling error and measurement noise. A rigorous study of the systematic modeling errors and their effect on the image quality is required. With improvements in modeling accuracy, and with an increased number of measurements, we

expect to improve the image contrast-to-noise ratio to facilitate characterization of smaller lesions. Currently, we have only two wavelengths of data and are not able to simultaneously determine the content of water and lipid, as well as oxygenated and deoxygenated hemoglobin. We are therefore developing an instrument with six wavelengths to improve the spectroscopic analysis. In our clinical trial, we noticed the heterogeneous nature of the breast, i.e., significant differences exist in the optical properties of fatty tissue and fiberglandular tissue. We also noticed that scattering carries useful information; ignoring scattering will potentially result in image errors. Since this is a very preliminary clinical trial and our goal is to reconstruct some reliable contrast first and also to determine the improvements that we must make in the future instruments and clinical trial, rather than try to extend it to quantitative and physiological study, we kept the data analysis simple and currently reconstruct absorption only. The results regarding the heterogeneous structure of the breast and scattering imaging results will be explored in the future with a modified system guided by these initial pilot results.

Our initial pilot clinical results demonstrated the feasibility of applying DOT simultaneously with digital x-ray tomosynthesis for breast lesion detection. With further development and validation of this methodology, we expect that this synergistic combination of optical functional information combined with x-ray structural information will play an important role in the clinical diagnosis of breast lesions and monitoring the response to therapy.

References

1. A. Yodh and B. Chance, "Spectroscopy and imaging with diffusing light," *Phys. Today* **48**, 34–40 (1995).
2. S. R. Arridge, "Optical tomography in medical imaging," *Inverse Probl.* **15**, R41–R93 (1999).
3. R. L. Barbour, H. L. Graber, J. Chang, S. S. Barbour, P. C. Koo, and R. Aronson, "MRI-guided optical tomography:prospects and computation for a new imaging method," *IEEE Comput. Sci. Eng.* **2**, 63–77 (1995).
4. S. Fantini, M. A. Franceschini, G. Gaida, H. Jess, H. Erdl, W. W. Mantulin, E. Gratton, K. T. Moesta, P. M. Schlag, and M. Kaschke, "Contrast-enhancement by edge effect corrections in frequency-domain optical mammography," in *OSA Trends in Optics and Photonics on Advances in Optical Imaging and Photon Migration*, Vol. 2, R. R. Alfano and J. G. Fujimoto, Eds., pp. 160–163, Optical Society of America, Washington, DC (1996).
5. S. B. Colak, M. B. van der Mark, G. W. Hooft, J. H. Hoogenraad, E. S. van der Linden, and F. A. Kuijpers, "Clinical optical tomography and NIR spectroscopy for breast cancer detection," *IEEE J. Sel. Top. Quantum Electron.* **5**, 1143–1158 (1999).
6. B. W. Pogue, S. P. Poplack, T. O. McBride, W. A. Wells, K. S. Osterman, U. L. Osterberg, and K. D. Paulsen, "Quantitative hemoglobin tomography with diffuse near-infrared spectroscopy: pilot results in the breast," *Radiology* **218**, 261–266 (2001).
7. H. B. Jiang, N. V. Iftimia, Y. Xu, J. A. Eggert, L. L. Fajardo, and K. L. Klove, "Near-infrared optical imaging of the breast with model-based reconstruction," *Acad. Radiol.* **9**, 186–194 (2002).
8. A. E. Cerussi, A. J. Berger, F. Bevilacqua, N. Shah, D. Jakubowski, J. Butler, R. F. Holcombe, and B. J. Tromberg, "Sources of absorption and scattering contrast for near-infrared optical mammography," *Acad. Radiol.* **8**, 211–218 (2001).

9. M. Cutler, "Transillumination as an aid in the diagnosis of lesions," *Surg. Gynecol. Obstet.* **48**, 721–730 (1929).

10. A. Alveryd, I. Andersson, K. Aspegren, G. Balldin, N. Bjurstam, G. Edstrom, G. Fagerberg, U. Glas, O. Jarlman, S. Larsson, E. Lidbrink, H. Lingaas, M. Lofgren, C. Rudenstam, L. Strender, L. Samuelsson, L. Tabar, A. Taube, H. Wallberg, P. Akesson, and D. Hallberg, "Lightscanning versus mammography for the detection of breast cancer in screening and clinical practice. A Swedish multicenter study," *Cancer* **65**, 1671–1677 (1990).

11. S. Chandrasekhar, *Radiative Transfer*, Dover, New York (1960).

12. A. E. Cerussi, D. Jakubowski, N. Shah, F. Bevilacqua, R. Lanning, A. J. Berger, D. Hsiang, J. Butler, R. F. Holcombe, and B. J. Tromberg, "Spectroscopy enhances the information content of optical mammography," *J. Biomed. Opt.* **7**, 60–71 (2002).

13. T. Durduran, R. Choe, J. P. Culver, L. Zubkov, M. J. Holboke, J. Giammarco, B. Chance, and A. G. Yodh, "Bulk optical properties of healthy female breast tissue," *Phys. Med. Biol.* **47**, 2847–2861 (2002).

14. M. A. Franceschini, K. T. Moesta, S. Fantini, G. Gaida, E. Gratton, H. Jess, W. W. Mantulin, M. Seeber, P. M. Schlag, and M. Kaschke, "Frequency-domain techniques enhance optical mammography: initial clinical results," *Proc. Natl. Acad. Sci. U.S.A.* **94**, 6468–6473 (1997).

15. B. Chance, "Near-infrared images using continuous, phase-modulated, and pulsed light with quantitation of blood and blood oxygenation," *Adv. Opt. Biop. Opt. Mammogr. Ann N.Y. Acad. Sci.* **838**, 19–45 (1998).

16. B. Chance, "Near-infrared images using continuous, phase-modulated, and pulsed light with quantitation of blood and blood oxygenation," in *Advances in Optical Biopsy and Optical Mammography*, Vol. 838, 29–45, Annals of the New York Academy of Sciences, New York (1998).

17. S. Fantini, S. A. Walker, M. A. Franceschini, M. Kaschke, P. M. Schlag, and K. T. Moesta, "Assessment of the size, position, and optical properties of breast tumors in vivo by noninvasive optical methods," *Appl. Opt.* **37**, 1982–1989 (1998).

18. D. Grosenick, H. Wabnitz, H. H. Rinneberg, K. T. Moesta, and P. M. Schlag, "Development of a time-domain optical mammograph and first in vivo applications," *Appl. Opt.* **38**, 2927–2943 (1999).

19. A. E. Cerussi, D. Jakubowski, N. Shah, F. Bevilacqua, R. Lanning, A. J. Berger, D. Hsiang, J. Butler, R. F. Holcombe, B. J. Tromberg, and G. Tsoucaris, "Spectroscopy enhances the information content of optical mammography," *J. Biomed. Opt.* **7**, 60–71 (2002).

20. B. J. Tromberg, N. Shah, R. Lanning, A. Cerussi, J. Espinoza, T. Pham, L. Svaasand, and J. Butler, "Non-invasive in vivo characterization of breast tumors using photon migration spectroscopy," *Neoplasia* **2**, 26–40 (2000).

21. A. Torricelli, L. Spinelli, A. Pifferi, P. Taroni, R. Cubeddu, and G. M. Danesini, "Use of a nonlinear perturbation approach for in vivo breast lesion characterization by multi-wavelength time-resolved optical mammography," *Opt. Express* **11**, 853–867 (2003).

22. S. Srinivasan, B. W. Pogue, S. D. Jiang, H. Dehghani, C. Kogel, S. Soho, J. J. Gibson, T. D. Tosteson, S. P. Poplack, and K. D. Paulsen, "Interpreting hemoglobin and water concentration, oxygen saturation, and scattering measured in vivo by near-infrared breast tomography," *Proc. Natl. Acad. Sci. U.S.A.* **100**, 12349–12354 (2003).

23. H. Dehghani, B. W. Pogue, S. P. Poplack, and K. D. Paulsen, "Multiwavelength three-dimensional near-infrared tomography of the breast: initial simulation, phantom, and clinical results," *Appl. Opt.* **42**, 135–145 (2003).

24. V. E. Pera, E. L. Heffer, H. Siebold, O. Schutz, S. Heywang-Kobrunner, L. Gotz, A. Heinig, and S. Fantini, "Spatial second-derivative image processing: an application to optical mammography to enhance the detection of breast tumors," *J. Biomed. Opt.* **8**, 517–524 (2003).

25. D. Grosenick, K. T. Moesta, H. Wabnitz, J. Mucke, C. Stroszczynski, R. Macdonald, P. M. Schlag, and H. Rinneberg, "Time-domain optical mammography: initial clinical results on detection and characterization of breast tumors," *Appl. Opt.* **42**, 3170–3186 (2003).

26. J. P. Culver, R. Choe, M. J. Holboke, L. Zubkov, T. Durduran, A. Slemp, V. Ntziachristos, B. Chance, and A. G. Yodh, "Three-dimensional diffuse optical tomography in the parallel plane transmission geometry: evaluation of a hybrid frequency domain/continuous wave clinical system for breast imaging," *Med. Phys.* **30**, 235–247 (2003).

27. R. L. Barbour, H. L. Graber, Y. L. Pei, S. Zhong, and C. H. Schmitz, "Optical tomographic imaging of dynamic features of dense-scattering media," *J. Opt. Soc. Am. A* **18**, 3018–3036 (2001).

28. D. J. Hawrysz and E. M. Sevick-Muraca, "Developments toward diagnostic breast cancer imaging using near-infrared optical measurements and fluorescent contrast agents," *Neoplasia* **2**, 388–417 (2000).

29. X. Intes, J. Ripoll, Y. Chen, S. Nioka, A. G. Yodh, and B. Chance, "In vivo continuous-wave optical breast imaging enhanced with indocyanine green," *Med. Phys.* **30**, 1039–1047 (2003).

30. Q. Zhu, E. Conant, and B. Chance, "Optical imaging as an adjunct to sonograph in differentiating benign from malignant breast lesions," *J. Biomed. Opt.* **5**, 229–236 (2000).

31. Q. I. Zhu, M. M. Huang, N. G. Chen, K. Zarfos, B. Jagjivan, M. Kane, P. Hedge, and S. H. Kurtzman, "Ultrasound-guided optical tomographic imaging of malignant and benign breast lesions: initial clinical results of 19 cases," *Neoplasia* **5**, 379–388 (2003).

32. V. Ntziachristos, A. G. Yodh, M. Schnall, and B. Chance, "Concurrent MRI and diffuse optical tomography of breast after indocyanine green enhancement," *Proc. Natl. Acad. Sci. U.S.A.* **97**, 2767–2772 (2000).

33. L. Tabar, G. Fagerberg, S. Duffy, N. Day, A. Gad, and O. Grontoft, "Update of the Swedish two-county program of mammographic screening for breast cancer," *Radiol. Clin. North Am.* **30**, 187–210 (1992).

34. L. Tabar, A. Gad, L. Holmberg, U. Ljungquist, G. Eklund, C. Fagerberg, L. Baldetorp, O. Grontoft, B. Lundstrom, J. Manson, N. Day, and F. Pettersson, "Reduction in mortality from breast cancer after mass screening with mammography," *Lancet* **1**, 829–832 (1985).

35. A. B. Miller, T. To, C. J. Baines, and C. Wall, "Canadian National Breast Screening Study—2: 13-year results of a randomized trial in women aged 50–59 years," *J. Natl. Cancer Inst. (1940-1978)* **92**, 1490–1499 (2000).

36. W. E. Barlow, C. D. Lehman, Y. Zheng, R. Ballard-Barbash, B. C. Yankaskas, G. R. Cutter, P. A. Carney, B. M. Geller, R. Rosenberg, K. Kerlikowske, D. L. Weaver, and S. H. Taplin, "Performance of diagnostic mammography for women with signs or symptoms of breast cancer," *J. Natl. Cancer Inst. (1940-1978)* **94**, 1151–1159 (2002).

37. S. Fletcher, W. Black, R. Harris, B. Rimer, and S. Shapiro, "Report of the International Workshop on Screening for Breast Cancer," *J. Non-Equilib. Thermodyn.* **85**, 1644–1656 (1993).

38. D. B. Kopans, *Breast Imaging*, Lippincott-Raven, New York (1998).

39. M. Sabel and H. Aichinger, "Recent developments in breast imaging," *Phys. Med. Biol.* **41**, 315–368 (1996).

40. Y. S. Yang, H. L. Liu, X. D. Li, and B. Chance, "Low-cost frequency-domain photon migration instrument for tissue spectroscopy, oximetry, and imaging," *Opt. Eng.* **36**, 1562–1569 (1997).

41. B. Chance, M. Cope, E. Gratton, N. Ramanujam, and B. Tromberg, "Phase measurement of light absorption and scatter in human tissue," *Rev. Sci. Instrum.* **69**, 3457–3481 (1998).

42. T. Wu, A. Stewart, M. Stanton, T. McCauley, W. Phillips, D. B. Kopans, R. H. Moore, J. W. Eberhard, B. Opsahl-Ong, L. Niklason, and M. B. Williams, "Tomographic mammography using a limited number of low-dose cone-beam projection images," *Med. Phys.* **30**, 365–380 (2003).

43. T. Wu, "Three dimensional mammography reconstruction using low-dose projection images," PhD Thesis, School of Physics, Brandeis University, Waltham (2002).

44. M. A. O'Leary, "Imaging with diffuse photon density waves," PhD Thesis, Department of Physics, University of Pennsylvania, Philadelphia (1996).

45. K. M. Yoo, F. Liu, and R. R. Alfano, "When does the diffusion approximation fail to describe photon transport in random media?" *Phys. Rev. Lett.* **64**, 2647–2650 (1992).

46. M. Born and E. Wolf, *Principles of Optics*, 7th ed., Cambridge University Press, Cambridge, UK (1999).

47. D. Boas, "Diffuse photon probes of structural and dynamical properties of turbid media: theory and biomedical applications," PhD Thesis, Department of Physics, University of Pennsylvania, Philadelphia (1996).

48. R. J. Gaudette, D. H. Brooks, C. A. DiMarzio, M. E. Kilmer, E. L. Miller, T. Gaudette, and D. A. Boas, "A comparison study of linear reconstruction techniques for diffuse optical tomographic imaging of absorption coefficient [in process citation]," *Phys. Med. Biol.* **45**, 1051–1070 (2000).

49. A. C. Kak and M. Slaney, *Principles of Computerized Tomographic Imaging*, IEEE Press, New York (1988).

50. W. H. Press, S. A. Teukolsky, W. T. Vetterling, and B. P. Flannery, *Numerical Recipes in C: The Art of Scientific Computing*, Cambridge University Press, Cambridge, UK (1997).

51. A. N. Tikhonov, *Solutions of Ill-Posed Problems*, Halsted Press, New York (1977).

52. P. C. Hansen, *Rank-Deficient and Discrete Ill-Posed Problems*, SIAM, Philadelphia (1998).

53. R. L. Barbour, H. L. Graber, J. W. Chang, S. L. S. Barbour, P. C. Koo, and R. Aronson, ''MRI-guided optical tomography: prospects and computation for a new imaging method,'' *IEEE Comput. Sci. Eng.* **2**, 63–77 (1995).

54. Q. Zhu, T. Durduran, V. Ntziachristos, M. Holboke, and A. G. Yodh, ''Imager that combines near-infrared diffusive light and ultrasound,'' *Opt. Lett.* **24**, 1050–1052 (1999).

55. V. Ntziachristos, A. G. Yodh, M. D. Schnall, and B. Chance, ''MRI-guided diffuse optical spectroscopy of malignant and benign breast lesions,'' *Neoplasia* **4**, 347–354 (2002).

56. B. A. Brooksby, H. Dehghani, B. W. Pogue, and K. D. Paulsen, ''Near-infrared (NIR) tomography breast image reconstruction with a priori structural information from MRI: algorithm development for reconstructing heterogeneities,'' *IEEE J. Sel. Top. Quantum Electron.* **9**, 199–209 (2003).

57. S. R. Arridge and M. Schweiger, ''Inverse methods for optical tomography,'' in *Information Processing in Medical Imaging 13th International Conference, IPMI'93 Flagstaff, Arizona, U.S.A., June 14-18, 1993 Proceedings (Lecture Notes in Computer Science)* , Vol. 687, pp. 259–277, Springer-Verlag, New York (1993).

58. B. W. Pogue, T. O. McBride, J. Prewitt, U. L. Osterberg, and K. D. Paulsen, ''Spatially variant regularization improves diffuse optical tomography,'' *Appl. Opt.* **38**, 2950–2961 (1999).

59. A. Li, E. L. Miller, M. E. Kilmer, T. J. Brukilacchio, T. Chaves, J. Stott, Q. Zhang, T. Wu, M. Chorlton, R. H. Moore, D. B. Kopans, and D. A. Boas, ''Tomographic optical breast imaging guided by three-dimensional mammography,'' *Appl. Opt.* **42**, 5181–5190 (2003).

60. D. A. Boas, T. Gaudette, and S. R. Arridge, ''Simultaneous imaging and optode calibration with diffuse optical tomography,'' *Opt. Express* **8**, 263–270 (2001).

61. M. J. Eppstein, D. J. Hawrysz, A. Godavarty, and E. M. Sevick-Muraca, ''Three-dimensional, Bayesian image reconstruction from sparse and noisy data sets: near-infrared fluorescence tomography,'' *Proc. Natl. Acad. Sci. U.S.A.* **99**, 9619–9624 (2002).